

IFS DOCUMENTATION – Cy48r1
Operational implementation 27 June 2023

**PART V: ENSEMBLE PREDICTION
SYSTEM**

© Copyright 2020-

European Centre for Medium-Range Weather Forecasts
Shinfield Park, Reading, RG2 9AX, UK

The content of this document is available for use under a Creative Commons Attribution 4.0 International Public License. See the terms at <https://creativecommons.org/licenses/by/4.0>.

REVISION HISTORY

Changes since CY43R1

- Chapter 2. Update to gamma value.

Changes since CY41R2

- Chapter Methodology sections updated: Introduction.
- Chapter Computational details - initial perturbations : gamma values updated in section, Initial perturbation component based on singular vectors.
- Equation 1.3 corrected.

Chapter 1

Methodology

Table of contents

- [1.1 Introduction](#)
- [1.2 Initial condition perturbations](#)
- [1.3 Singular vectors](#)
 - [1.3.1 Formulation of the singular vector computation](#)
 - [1.3.2 Use of the total energy norm](#)
 - [1.3.3 Use of the Hessian of the 3D-Var objective function](#)
- [Appendix A. Eigenvalue algorithms](#)
 - [A.1 The Lanczos algorithm](#)
 - [A.2 The Jacobi–Davidson algorithm](#)
 - [A.3 Solution method](#)

1.1 INTRODUCTION

Ensemble prediction is a method to predict the probability distribution of forecast states, given a probability distribution of random analysis error and model uncertainties. In ensemble systems, the impact of analysis and model uncertainties on forecasts states are simulated by starting the ensemble of forecasts from different initial conditions, and computing each forecast evolution using schemes designed to simulate model uncertainties. Since 1992, ensemble prediction systems have been part of the operational forecasting suite at ECMWF ([Palmer *et al.*, 1993](#)) and NCEP ([Toth and Kalnay, 1993, 1997](#)). A general description of the first version of the ECMWF EPS can be found in [Molteni *et al.* \(1996\)](#), and more recent versions of the operational ensemble forecasts are described by [Leutbecher and Palmer \(2008\)](#) and [Lang *et al.* \(2021\)](#).

The implementations by ECMWF and NCEP in the early 90-s were followed in 1995 by MSC Canada ([Houtekamer *et al.*, 1996b,a](#)) and in 1998 by BoM Australia. The reader is referred to [Buizza *et al.* \(2005\)](#) for a comparison of the performance of the ECMWF, MSC and NCEP ensemble systems over the northern hemisphere, and to [Bourke *et al.* \(2005\)](#) for a comparison of the performance of the ECMWF and the BoM systems over the southern hemisphere. In the past decade, other meteorological centres have started producing routinely ensemble-based probabilistic forecasts, see for example [Park *et al.* \(2008\)](#) for comparison of the performance of eight global ensemble prediction systems archived within the TIGGE project. The reader is referred to [Hagedorn *et al.* \(2012\)](#) for a more recent comparison of the performance of the ECMWF EPS and multi-model ensemble systems defined by the TIGGE ensembles.

The atmospheric model IFS is coupled from initial time to the ocean model NEMO (see [Madec, 2008](#)). The coupling uses the single executable framework described by [Mogensen *et al.* \(2012b\)](#). The ocean initial conditions come from the near-real-time component of the operational ocean analysis (NEMOVAR, see [Mogensen *et al.*, 2012a](#)) and from the Ocean ReAnalysis System 5 (ORAS5, see [Zuo *et al.*, 2017](#)) for re-forecasts. Further details on the coupling are given in [3.1](#).

The 50+1 medium-range non-linear integrations from day 0 to day 15 have a resolution of TCo1279. They are initialised twice daily at 00 and 12 UTC. In addition, 100+1 extended-range integrations from day 0 to day 46 are initialised at 00 UTC daily with a resolution of TCo319. In the vertical, all integrations have 137 levels, with the model top at 1 Pa. The extended-range integrations start from $t = 0$ h since 27 June 2023. The two separate ensembles for medium-range and extended-range supersede a variable-resolution system, which was operational from 12 September 2006 (VAREPS, see [Buizza *et al.* \(2007\)](#)) to

27 June 2023. Earlier configurations of the extended-range/monthly ensemble are described by Vitart (2004) and Vitart *et al.* (2008). The separation into two separate ensembles has the following advantages: (i) it made it feasible to double the ensemble size for the extended-range forecasts from 50 to 100 perturbed members, (ii) it provides more flexibility for future revisions of the re-forecasts (see below), and (iii) it permits users to generate dual-resolution ensemble forecast products based on 150 members for the medium-range (Leutbecher and Ben Bouallègue, 2020; Baran *et al.*, 2019).

On 11 March 2008, a new ensemble re-forecast suite was implemented to estimate the model climatological distribution (see Hagedorn, 2008 for a description of the system). Since 27 June 2023, there are two reforecast suites for the medium-range and extended-range. Their resolutions are TCo1279 and TCo319, respectively, in order to match the resolutions of the real-time forecasts. Both re-forecast suites consist of 11-member ensembles, integrated with the same model version used in the real-time forecasts, and run twice weekly (on Mondays and Thursdays) for the same calendar day over the past 20 years (in 2023, from 2003 to 2022). Thus, 440 ensemble members $((11 + 11) \times 20)$ are available per week for each resolution to estimate the respective model climatology and to calibrate the forecasts. The initial conditions for the re-forecasts are defined by ERA5 analyses (Hersbach *et al.*, 2019; Vitart *et al.*, 2019). Re-forecasts are used to generate some operational medium-range (e.g. the Extreme Forecast Index) and monthly products.

The first EPS configurations were designed on the notion that forecast uncertainty is dominated by error or uncertainty in the initial conditions (see Harrison *et al.*, 1999). This was consistent with studies that show that, when two operational forecasts differ, it is usually differences in the analyses rather than differences in model formulation that are critical to explaining this difference. Later on it was recognized that random model errors due to physical parameterizations and the effects of subgrid-scale processes could affect the forecast quality too. Model uncertainties are represented in the EPS with the Stochastically Perturbed Parameterization Tendencies scheme (SPPT). It simulates the effect on forecast uncertainty of random model errors due to the parametrized physical processes.

The SPPT scheme was first implemented in October 1998 and referred to originally as *stochastic physics* (Buizza *et al.*, 1999b). The scheme perturbs the tendencies by terms that are given by a random pattern times the net parameterized physics tendencies less the diagnosed clear-sky heating rate. The random pattern varies horizontally and with time; each ensemble member uses a different realisation of the random pattern. Three major revisions of the SPPT scheme took place in September 2009 (Palmer *et al.*, 2009), in November 2010 and in June 2018. As in the original scheme, tendency perturbations are given by a multiplicative noise term based on the net parameterized physics tendencies. In the revised SPPT scheme, the random pattern that defines the perturbations varies smoothly in space and time in contrast to the original scheme. The random numbers at a grid point are given by a truncated Gaussian distribution. The pattern is defined as the sum of three independent random patterns with horizontal correlation scales of 500, 1000 and 2000 km and correlation time scales of 6 h, 3 d and 30 d, respectively. The standard deviation of the three patterns decreases with increasing spatial and temporal scale from 0.42 to 0.14 and finally to 0.048. In November 2016, a global constraint was introduced in SPPT that modifies the perturbations in such a way that the global integral of the perturbed physics tendency is equal to the global integral of the unperturbed physics tendency (Leutbecher *et al.*, 2017). This global constraint reduces the precipitation minus evaporation imbalance generated by lack of humidity conservation in SPPT. In June 2018, the diagnosed clear-sky heating rate was removed from the net tendency that is perturbed by SPPT (Lock *et al.*, 2019). This was done to avoid the strong diurnal cycle of the tendency perturbations documented by Leutbecher *et al.* (2017). In addition, the standard deviation of the random pattern was reduced by 20% to the current values in order to avoid overdispersion in the tropics in general and for the MJO in particular.

The Stochastic Kinetic Energy Backscatter scheme (SKEB) used from November 2010 to May 2018 has been deactivated. SKEB had been used to introduce perturbations to simulate the unresolved upscale transfer of energy from sub-grid scales to the resolved scales, by introducing a stochastic streamfunction forcing (Berner *et al.*, 2009). The most recent model configurations showed that SKEB contributes little additional skill beyond the improvements obtained with SPPT (Leutbecher *et al.*, 2017).

There are two key advantages of using ensemble-based probabilistic forecasts instead of single forecasts. Firstly, they provide a more complete estimation of the future forecast states, since they not only provide

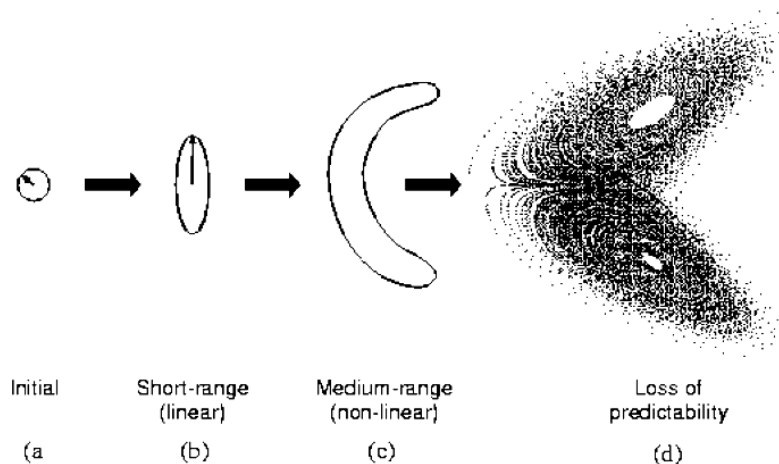


Figure 1.1 A schematic illustration of the growth of an isopleth of the forecast error probability distribution function, from (a) initial phase, to (b) linear growth phase, to (c) nonlinear growth phase, to (d) loss of predictability. See text for further details.

the most likely scenario but also the probability that alternatives might occur. Secondly, they provide more consistent forecasts (Zsoter *et al.*, 2009). Fig. 1.1 shows a schematic illustration of the phase-space evolution of the probability distribution function (PDF) of analysis error throughout the forecast range. A specific isopleth (e.g. the 1 standard deviation isopleth) is illustrated. It is assumed that the initial time PDF is a Gaussian distribution. At initial time (Fig. 1.1(a)), the isopleth is shown as isotropic, i.e. bounding an n -sphere, where the dimension of phase space n is of the order of ($O(10^9)$) for the ECMWF operational forecast model). In general, this error will not be isotropic—analysis error is likely to be larger along directions which are less well observed, and vice versa. However, at least in principle, it is straightforward to define an inner product on phase space, with respect to which the initial PDF is isotropic. This inner product, defined from the analysis error covariance matrix, plays a fundamental role in the theory of singular vectors discussed below.

In the early part of the forecast, error growth is governed by linear dynamics. During this period an initially spherical isopleth of the PDF will evolve to bound an n -dimensional ellipsoidal volume (Fig. 1.1(b)). The major axis of the ellipsoid corresponds to a phase-space direction which defines the dominant finite-time instability of that part of phase space (relative to the analysis error covariance metric). The arrow shown in Fig. 1.1(b) points along the major axis of the ellipsoid. It can be thought of as evolving from the arrow shown in Fig. 1.1(a). Note that the arrows in Fig. 1.1(a) and Fig. 1.1(b) are not parallel to one another. This illustrates the non-modal nature of linear perturbation growth.

The arrows at initial and forecast time define the dominant singular vector at initial and final time (with respect to the analysis error covariance metric). At forecast time, the dominant singular vector defines the dominant eigenvector of the forecast error covariance matrix. See Section 1.3.1 for more details.

The growth of the (isopleth of the) PDF between Fig. 1.1(b) and Fig. 1.1(c) describes a nonlinear evolution of the PDF. In Figs 1.1(c) the PDF has deformed from its ellipsoidal shape in Fig. 1.1(b). The nonlinear deformation will cause the PDF to evolve away from a Gaussian distribution. Put another way, in the nonlinear phase, the PDF in any given direction is partially determined by perturbations which, in the linear phase, were orthogonal to that direction. Finally, Fig. 1.1(d) shows (schematically) the situation where the evolved PDF has effectively become indistinguishable from the system's attractor, so that all predictability has been lost.

1.2 INITIAL CONDITION PERTURBATIONS

The operational EPS samples initial uncertainty using perturbations from an ensemble of data assimilations (EDA) and perturbations constructed from the leading singular vectors since June 2010.

The perturbations from the EDA replace the perturbations that were based on evolved singular vectors prior to June 2010.

The observed values are perturbed with stochastic noise in the EDA. The variance of the observation perturbations is given by the observation error variance estimate that is used in the data assimilation. In addition, model uncertainties are represented in the EDA using the SPPT scheme. The EDA consists of 50 perturbed analyses with an outer loop resolution of $T_{C_0}639$. Further details about the data assimilation system and the EDA are provided in Part II of the IFS documentation and by [Isaksen *et al.* \(2010\)](#). The EDA also provides the operational high-resolution 4D-Var with an estimate of the flow-dependent variations of the background error variances.

If all relevant sources of uncertainty were represented accurately in the EDA, it should provide a reliable sample from the distribution of initial uncertainties. Ensemble prediction experiments using only EDA initial perturbations indicate that this goal has not been achieved yet. Therefore, [Buizza *et al.* \(2008\)](#) propose the hybrid approach of combining EDA perturbations with singular vector perturbations. The perturbations from the EDA sample errors that have grown in the past while the perturbations based on singular vectors sample structures that are likely to dominate forecast error in the future, say at Day 2 and beyond.

1.3 SINGULAR VECTORS

The number of degrees of freedom of the operational ECMWF model is many orders of magnitude larger than the largest practicable ensemble size. This raises the question of whether any particular strategy is desirable in sampling the initial PDF. If initial errors can occur independently in all the phase-space directions, then a strategy of random-under-sampling could lead to an EPS whose reliability was poor, especially for cases of small ensemble spread. In particular, if the spread from a randomly under-sampled ensemble was found to be small on a particular occasion, this could either be because the flow was especially predictable, or because the ensemble perturbations poorly sample the unstable subspace in which the analysis error lay. From a credibility perspective, it is important to try to minimize the latter type of occurrence.

An alternative strategy is to base the perturbations on the leading singular vectors. Clearly, by focusing on the unstable subspace, the cases of small spread being associated with large forecast error should be minimized, at least in the linear and weakly nonlinear range. In addition to this, there are several related reasons why the initial perturbations for the ECMWF EPS are based on the dominant singular vectors.

Firstly, as shown by [Rabier *et al.* \(1996\)](#) and [Gelaro *et al.* \(1998\)](#), the sensitivity of day-2 forecast error to perturbations in the initial state projects well into the space of dominant singular vectors. Rabier *et al.* have shown that cases of severe forecast failure can be dramatically improved if the analysis is modified using the sensitivity perturbations.

Secondly, provided the metric or inner product for the singular vectors is an accurate reflection of the analysis error covariance matrix then, as mentioned, the evolved singular vectors point along the largest eigenvectors of the forecast error covariance matrix. As such (see [Ehrendorfer and Tribbia, 1997](#)), perturbations constructed from the dominant singular vectors represent the most efficient means for predicting the forecast error covariance matrix, given a pre-specified number of allowable tangent model integrations.

Thirdly, singular vector perturbations may provide a relatively efficient means of sampling the forecast error PDF in the nonlinear range, particularly during transitions in weather regimes. For example, [Mureau *et al.* \(1993\)](#) have shown a case where the singular vector perturbations were successful in capturing a major transition to blocking, where random perturbations were inadequate. [Gelaro *et al.* \(1998\)](#) have documented further such cases. A more systematic study of the ability of ensembles to describe the probability of regime transitions in the weakly nonlinear forecast range has been made by [Trevisan *et al.* \(2001\)](#) using an intermediate-complexity model of the extratropical circulation. Relatively small ensembles initialised using firstly singular vectors, and secondly local Lyapunov vectors, were compared with a large Monte-Carlo ensemble based on random perturbations. It was found that small ensemble spread from the singular-vector ensemble was a reliable indicator of

small ensemble spread from the Monte-Carlo ensemble. By contrast, small ensemble spread from the Lyapunov-vector ensemble was a much less reliable indicator of small spread from the Monte-Carlo ensemble.

Fourthly, in practice only imperfect information about the initial PDF is available. Hence it is difficult to even define a truly random initial sampling.

In the current system, each EPS perturbation is a linear combination of singular vectors with maximum growth computed using a total energy norm, over a 48 hour time period. The leading 50 singular vectors are used for each extra-tropical hemisphere, and the leading 5 singular vectors are used in each of up to 6 tropical areas. They are computed at T42 resolution and with 137 vertical levels. The assumption underlying the linear combination is that initial error is distributed in the space spanned by the singular vectors according to an isotropic Gaussian distribution. A Gaussian sampling technique is used to sample realisations from this distribution (see [Leutbecher and Palmer \(2008\)](#) and [Section 2.3](#)).

The reader is referred to [Buizza and Palmer \(1995\)](#) for a description of the singular vector computation in the extra-tropics, and to [Barkmeijer et al. \(2001\)](#) for a discussion of the computation of the tropical singular vectors. The reader is also referred to [Palmer et al. \(1998\)](#) for a discussion of the sensitivity of the singular vector structure to the metric used to measure perturbation growth, to [Hoskins et al. \(2000\)](#) for an analysis of the nature of singular vector growth, and to [Barkmeijer et al. \(1998\)](#) and [Lawrence et al. \(2009\)](#) for comparisons of singular vectors computed using a total energy metric and singular vectors based on a Hessian metric. [Leutbecher and Lang \(2014\)](#) study the reliability of ensemble variances in subspaces spanned by the leading singular vectors. They also examine the sensitivity of this reliability to the dimension of the singular vector subspace and the horizontal resolution of the singular vectors.

1.3.1 Formulation of the singular vector computation

One way to define singular vectors is by means of a maximization problem. The scalar which has to be maximized can be written as

$$\frac{[\mathbf{E}\mathbf{x}, \mathbf{M}\mathbf{x}]}{[\mathbf{D}\mathbf{x}, \mathbf{x}]} \quad (1.1)$$

where $[\cdot, \cdot]$ denotes the Euclidean inner product, $[\mathbf{x}, \mathbf{y}] = \sum(x_i y_i)$, and \mathbf{D} and \mathbf{E} are positive definite operators. The operator \mathbf{M} is the propagator of the tangent model. It assigns to a particular vector \mathbf{x} the linearly evolved vector $\mathbf{M}\mathbf{x}$ for a given forecast time and with respect to a reference trajectory. Hence, the scalar defined by (1.1) is the ratio between the \mathbf{E} -norm of the evolved vector \mathbf{x} and the \mathbf{D} -norm of \mathbf{x} at initial time. Notice that the norm at initial and final time may differ. The leading singular vector has the property that it maximizes the scalar, the second singular vector maximizes the scalar in the space \mathbf{D} -orthogonal to the leading singular vector, and so forth. In this way, one obtains a set of singular vectors which are \mathbf{D} -orthogonal at initial time and \mathbf{E} -orthogonal at final time. The actual computation of the singular vectors in the IFS is done by solving an equivalent eigenvalue problem. Observe that the solutions of the maximization problem (1.1) also satisfy the generalized eigenvalue problem (1.2) given by

$$\mathbf{M}^* \mathbf{E} \mathbf{M} \mathbf{x} = \lambda \mathbf{D} \mathbf{x} \quad (1.2)$$

where \mathbf{M}^* is the adjoint of \mathbf{M} . The defining equation (1.2) can be generalized by activating operators in the singular vector computation, see [Section 1.3](#). It is, for instance, possible to set the state vector to zero outside a prescribed area at optimization time, by using a projection operator \mathbf{P} ([Buizza, 1994](#)). Consequently, the growth of singular vectors outside the target area is not taken into account in the actual computation. In using this projection operator, the eigenvalue problem (1.2) becomes $\mathbf{M}^* \mathbf{P}^* \mathbf{E} \mathbf{P} \mathbf{M} \mathbf{x} = \lambda \mathbf{D} \mathbf{x}$. To keep the notation as simple as possible, these additional operators will be omitted from the basic eigenvalue problem (1.2).

The operator \mathbf{D} determines the properties by which the singular vectors are constrained at initial time. As such, it can be interpreted as an approximation of the inverse of the analysis error covariance matrix \mathbf{P}^a . Currently, there are two methods to compute singular vectors, depending on the form of \mathbf{D} . Both methods will be discussed in [Subsections 1.3.2](#) and [1.3.3](#).

1.3.2 Use of the total energy norm

When using the total energy norm, or any other simple operator, at initial time, the generalized eigenvalue problem (1.2) can be simplified to an ordinary eigenvalue problem. In this case the \mathbf{D} -norm of \mathbf{x} reads as

$$[\mathbf{x}, \mathbf{D}\mathbf{x}] = \frac{1}{2} \int_0^1 \int_{\Sigma} \left\{ -\Delta^{-1} \zeta_{\mathbf{x}} \cdot \zeta_{\mathbf{x}} - \Delta^{-1} D_{\mathbf{x}} \cdot D_{\mathbf{x}} + \frac{c_p}{T_{\text{ref}}} T_{\mathbf{x}}^2 + w_q \frac{L_{\text{cond}}^2}{c_p T_{\text{ref}}} q_{\mathbf{x}}^2 \right\} d\Sigma \frac{\partial p}{\partial \eta} d\eta + \frac{1}{2} \int_{\Sigma} R_{\text{dry}} T_{\text{ref}} P_{\text{ref}} \ln(\pi_{\mathbf{x}}) \ln(\pi_{\mathbf{x}}) d\Sigma \quad (1.3)$$

where $\zeta_{\mathbf{x}}$, $D_{\mathbf{x}}$, $T_{\mathbf{x}}$ and $\ln \pi_{\mathbf{x}}$ stand for the vorticity, divergence, temperature, specific humidity and logarithm of the surface pressure component of the state vector \mathbf{x} , and c_p is the specific heat of dry air at constant pressure, L_{cond} is the latent heat of condensation at 0°C , R_{dry} is the gas constant for dry air, $T_{\text{ref}} = 300\text{ K}$ is a reference temperature and $P_{\text{ref}} = 800\text{ hPa}$ is a reference pressure. The parameter w_q defines the relative weight given to the specific humidity term. The integration over the sphere and in the vertical are denoted by $\int_{\Sigma} d\Sigma$ and $\int_0^1 d\eta$, respectively.

Since the operator \mathbf{D} is a diagonal matrix, one can easily define a matrix \mathbf{C} so that $\mathbf{C}^2 = \mathbf{D}^{-1}$. Multiplying both sides of (1.2) to the left and right with \mathbf{C} , yields the equation

$$\mathbf{C}\mathbf{M}^*\mathbf{E}\mathbf{M}\mathbf{C}\mathbf{x} = \lambda \mathbf{x} \quad (1.4)$$

which can be solved using the Lanczos algorithm, see Section A.1. The energy metric is believed to be a useful approximation to the analysis error covariance metric (Palmer *et al.*, 1998).

1.3.3 Use of the Hessian of the 3D-Var objective function

In the incremental formulation of 3D-Var, the Hessian of the objective function \mathfrak{S} can be used as an approximation of the inverse of the analysis error covariance matrix. The objective function has the form

$$\mathfrak{S}(\delta\mathbf{x}) = \frac{1}{2} \delta\mathbf{x}^T \mathbf{B}^{-1} \delta\mathbf{x} + \frac{1}{2} (\mathbf{H}\delta\mathbf{x} - \mathbf{d})^T \mathbf{R}^{-1} (\mathbf{H}\delta\mathbf{x} - \mathbf{d}) \quad (1.5)$$

and the increment $\delta\mathbf{x}^a$ where \mathfrak{S} attains its minimum, provides the analysis \mathbf{x}^a which is defined by adding $\delta\mathbf{x}^a$ to the background \mathbf{x}^b so that

$$\mathbf{x}^a = \mathbf{x}^b + \delta\mathbf{x}^a \quad (1.6)$$

The operators \mathbf{B} and \mathbf{R} are covariance matrices of the background and observation error respectively and \mathbf{d} is the innovation vector given by

$$\mathbf{d} = \mathbf{y} - \mathbf{H}\mathbf{x}^b \quad (1.7)$$

where \mathbf{y} is the observation vector and \mathbf{H} is a linear approximation of the observation operator in the vicinity of \mathbf{x}^b .

The Hessian $\nabla\nabla\mathfrak{S}$ of the objective function is given by

$$\nabla\nabla\mathfrak{S} = \mathbf{B}^{-1} + \mathbf{H}^T \mathbf{R}^{-1} \mathbf{H} \quad (1.8)$$

Provided that the background error ($\mathbf{x}^b - \mathbf{x}^t$) and the observation error ($\mathbf{y} - \mathbf{H}\mathbf{x}^t$) are uncorrelated, with \mathbf{x}^t the true state of the atmosphere, the Hessian $\nabla\nabla\mathfrak{S}$ is equal to the inverse of the analysis error covariance matrix \mathbf{P}^a . This follows by noting that the objective function is quadratic and attains its unique minimum at $\delta\mathbf{x}^a$ and consequently, by using (1.6),

$$\mathbf{B}^{-1}[\mathbf{x}^a - \mathbf{x}^t - (\mathbf{x}^b - \mathbf{x}^t)] + \mathbf{H}^T \mathbf{R}^{-1} [\mathbf{H}(\mathbf{x}^a - \mathbf{x}^t) + \mathbf{H}\mathbf{x}^t - \mathbf{y}] = 0 \quad (1.9)$$

Rewriting (1.9) gives

$$(\mathbf{B}^{-1} + \mathbf{H}^T \mathbf{R}^{-1} \mathbf{H})(\mathbf{x}^a - \mathbf{x}^t) = \mathbf{B}^{-1}(\mathbf{x}^b - \mathbf{x}^t) - \mathbf{H}^T \mathbf{R}^{-1}(\mathbf{H}\mathbf{x}^t - \mathbf{y}) \quad (1.10)$$

Using the assumption that the background and observation error are uncorrelated the above equation implies that

$$(\mathbf{B}^{-1} + \mathbf{H}^T \mathbf{R}^{-1} \mathbf{H}) \mathbf{P}^a (\mathbf{B}^{-1} + \mathbf{H}^T \mathbf{R}^{-1} \mathbf{H})^T = (\mathbf{B}^{-1} + \mathbf{H}^T \mathbf{R}^{-1} \mathbf{H})^T \quad (1.11)$$

Now by multiplying each side of (1.11) to the right with its transpose, the desired result follows.

The defining eigenvalue problem for the singular vectors becomes

$$\mathbf{M}^* \mathbf{E} \mathbf{M} \mathbf{x} = \lambda \nabla \nabla \mathfrak{S} \mathbf{x} \quad (1.12)$$

Since the objective function is quadratic in the incremental formulation, the Hessian applied to a vector $\nabla \nabla \mathfrak{S} \mathbf{x}$ in (1.12) can be evaluated as finite difference of two gradients: $(\nabla \nabla \mathfrak{S}) \mathbf{x} = \nabla \mathfrak{S}(\mathbf{x} + \mathbf{x}^b) - \nabla \mathfrak{S}(\mathbf{x}^b)$. The generalized eigenvalue problem (1.12) is solved by using the Jacobi–Davidson algorithm, see Section A.2.

APPENDIX A. EIGENVALUE ALGORITHMS

A.1 The Lanczos algorithm

Algorithms based on Lanczos theory are very useful to solve an eigenvalue problem when only a few of the extreme eigenvectors are needed. It can be applied to large and sparse problems. The algorithm does not access directly the matrix elements of the operator that defines the problem, but it gives an estimate of the eigenvectors through successive application of the operator.

Consider the eigenvalue problem

$$\mathbf{A} \mathbf{x} = \sigma_i^2 \mathbf{x} \quad (A.1)$$

where the matrix \mathbf{A} is $N \times N$ dimensional, and symmetric. Without loss of generality, we can also suppose that it is real.

If \mathbf{A} is a real, symmetric matrix, then there exists an orthogonal real matrix \mathbf{Q} such that

$$\mathbf{Q}^T \mathbf{A} \mathbf{Q} = \mathbf{D}(\lambda_1, \dots, \lambda_N) \quad (A.2)$$

where $\mathbf{D}(\lambda_1, \dots, \lambda_2)$ is a diagonal matrix, and \mathbf{Q}^T denotes the transpose of \mathbf{Q} (Schur decomposition theorem).

The Lanczos algorithm does not directly compute the diagonal matrix \mathbf{D} , but it first computes a partial transformation of the matrix \mathbf{A} using a tridiagonal matrix \mathbf{T}

$$\mathbf{Q}^T \mathbf{A} \mathbf{Q} = \mathbf{T} \quad (A.3)$$

with

$$\mathbf{T} = \begin{bmatrix} \alpha_1 & \beta_2 & 0 & \cdot & \cdot & \cdot & \cdot \\ \beta_2 & \alpha_2 & \beta_3 & 0 & \cdot & \cdot & \cdot \\ 0 & \beta_3 & \cdot & \cdot & \cdot & \cdot & \cdot \\ \cdot & 0 & \cdot & \cdot & \cdot & 0 & \cdot \\ \cdot & \cdot & \cdot & \cdot & \cdot & \beta_{J-1} & 0 \\ \cdot & \cdot & \cdot & 0 & \beta_{J-1} & \alpha_{J-1} & \beta_J \\ \cdot & \cdot & \cdot & \cdot & 0 & \beta_J & \alpha_J \end{bmatrix} \quad (A.4)$$

and with

$$\mathbf{Q} = [\mathbf{q}_1, \dots, \mathbf{q}_J] \quad (A.5)$$

where the vectors \mathbf{q}_j are column vectors, and where the number of iterations J is much smaller than the dimensionality of the problem, $J \ll N$. Then, the Lanczos algorithm finds the diagonal decomposition of \mathbf{T}

$$\mathbf{T} = \mathbf{S}^T \mathbf{D} \mathbf{S} \quad (A.6)$$

The elements of the diagonal matrix \mathbf{D} are an estimate of the eigenvalues of \mathbf{A} , and an estimate of the eigenvectors are given by $\mathbf{Y} = [\mathbf{y}_1, \dots, \mathbf{y}_j]$, with

$$\mathbf{Y} = \mathbf{Q} \mathbf{S} \quad (A.7)$$

The actual computation is performed by writing (A.3) as

$$\mathbf{A}\mathbf{Q} = \mathbf{Q}\mathbf{T} \quad (\text{A.8})$$

Equating columns of (A.8), it follows that

$$\mathbf{A}\mathbf{q}_j = \beta_{j-1}\mathbf{q}_{j-1} + \alpha_j\mathbf{q}_j + \beta_j\mathbf{q}_{j+1} \quad (\text{A.9})$$

for $j = 1, \dots, J$. The orthogonality of the vectors \mathbf{q}_j implies that

$$\alpha_j = \mathbf{q}_j^T \mathbf{A} \mathbf{q}_j \quad (\text{A.10})$$

Moreover, if

$$\mathbf{r}_j = (\mathbf{A} - \alpha_j \mathbf{I}) \mathbf{q}_j - \beta_{j-1} \mathbf{q}_{j-1} \quad (\text{A.11})$$

is non-zero, then

$$\mathbf{q}_{j+1} = \frac{\mathbf{r}_j}{\beta_j} \quad (\text{A.12})$$

where $\beta_j = \pm \sqrt{\langle \mathbf{r}_j; \mathbf{r}_j \rangle}$. An iterative application of these equations, with a randomly chosen starting vector \mathbf{q}_1 , defines the Lanczos iterative procedure. The total number of iterations J determines the accuracy of the computation. As this number increases, more eigenpairs can be separated from the others, independently from the choice of the starting vector \mathbf{q} . This separation starts from the boundaries of the eigenvalue spectrum. The accuracy of the eigenvectors is less than the accuracy of the singular values, say to order ε when the precision of the singular values is of order ε^2 .

The reader is referred to [Golub and van Loan \(1983\)](#) for a theoretical description of the Lanczos algorithm. The Lanczos code is available in NAG issue 17. In the IFS, the Lanczos code in subroutine **CONGRAD** is used to compute the singular vectors used in the operational EPS.

A.2 The Jacobi–Davidson algorithm

The generalized eigenproblem

$$\mathbf{A}\mathbf{x} = \lambda\mathbf{B}\mathbf{x} \quad (\text{A.13})$$

is usually handled by bringing it back to a standard eigenproblem

$$\mathbf{B}^{-1}\mathbf{A}\mathbf{x} = \lambda\mathbf{x} \quad (\text{A.14})$$

The matrix $\mathbf{B}^{-1}\mathbf{A}$ is in general nonsymmetric, even if both \mathbf{A} and \mathbf{B} are symmetric. However, if \mathbf{B} is symmetric and positive definite, the \mathbf{B} -inner product is well defined. The matrix $\mathbf{B}^{-1}\mathbf{A}$ is symmetric in this inner product if \mathbf{A} is symmetric:

$$[\mathbf{w}, \mathbf{B}^{-1}\mathbf{A}\mathbf{v}]_{\mathbf{B}} = [\mathbf{B}\mathbf{w}, \mathbf{B}^{-1}\mathbf{A}\mathbf{v}] = [\mathbf{w}, \mathbf{A}\mathbf{v}] = [\mathbf{A}\mathbf{w}, \mathbf{v}] = [\mathbf{B}^{-1}\mathbf{A}\mathbf{w}, \mathbf{v}]_{\mathbf{B}} \quad (\text{A.15})$$

The proposed method to solve (A.14) constructs a set of basis vectors \mathbf{V} of a search space v , c.f. the Lanczos method. The approximate eigenvectors are linear combinations of the vectors \mathbf{V} . The classical and most natural choice for the search space v , for instance utilized in the Lanczos method, is the so-called Krylov subspace, the space spanned by the vectors

$$\mathbf{v}, \mathbf{B}^{-1}\mathbf{A}\mathbf{v}, (\mathbf{B}^{-1}\mathbf{A})^2\mathbf{v}, \dots, (\mathbf{B}^{-1}\mathbf{A})^{i-1}\mathbf{v} \quad (\text{A.16})$$

This i -dimensional subspace is denoted by $\mathbf{K}^i(\mathbf{v}, \mathbf{B}^{-1}\mathbf{A})$. The vector \mathbf{v} is a starting vector that has to be chosen. The Krylov subspace is well suited for computing dominant eigenpairs since the vector $(\mathbf{B}^{-1}\mathbf{A})^{i-1}\mathbf{v}$ points more and more in the direction of the dominant eigenvector of $\mathbf{B}^{-1}\mathbf{A}$ for increasing i .

Given a search space v , the approximate eigenpair (θ, \mathbf{u}) of (A.15) is a linear combination of the basis vectors of v so that

$$\mathbf{u} = \mathbf{V}\mathbf{y} \quad (\text{A.17})$$

A suitable criterion for finding an optimal pair is the Galerkin condition that the residual

$$\mathbf{r} = \mathbf{B}^{-1}\mathbf{A}\mathbf{u} - \theta\mathbf{u} = \mathbf{B}^{-1}\mathbf{A}\mathbf{V}\mathbf{y} - \theta\mathbf{V}\mathbf{y} \quad (\text{A.18})$$

is \mathbf{B} -orthogonal to the search space v . Hence

$$\mathbf{V}^T\mathbf{B}\mathbf{r} = 0 \quad (\text{A.19})$$

and consequently, using (A.19),

$$\mathbf{V}^T\mathbf{A}\mathbf{V}\mathbf{y} - \theta\mathbf{V}^T\mathbf{B}\mathbf{V}\mathbf{y} = 0 \quad (\text{A.20})$$

Note that the resulting eigenproblem is of the dimension of the search space, which is generally much smaller than of the original problem. The basis vectors are usually orthonormalized so that $\mathbf{V}^T\mathbf{B}\mathbf{V} = \mathbf{I}$. Approximate eigenpairs that adhere to the Galerkin condition are called Ritz pairs.

It can be shown that the residuals $\mathbf{r}_1, \mathbf{r}_2, \dots, \mathbf{r}_i$ form a \mathbf{B} -orthogonal basis for $\mathbf{K}^i(\mathbf{r}_1, \mathbf{B}^{-1}\mathbf{A})$ when the approximate eigenpairs are computed according to (A.17).

A.3 Solution method

As was stated before, the natural search space for the generalized eigenvalue problem is the Krylov subspace $\mathbf{K}^i(\mathbf{v}, \mathbf{B}^{-1}, \mathbf{A})$. This basis can be generated by expanding the basis by new residual vectors. The problem in the construction of a basis for this space is that operations with \mathbf{B}^{-1} are needed. Since in our application the inverse of \mathbf{B} is not known explicitly, its action is approximated by the Conjugate Residual method (CR). To compute the vector

$$\mathbf{r} = \mathbf{B}^{-1}\tilde{\mathbf{r}} \quad (\text{A.21})$$

one iteratively solves the system

$$\mathbf{B}\mathbf{r} = \tilde{\mathbf{r}} \quad (\text{A.22})$$

Iterative solution methods require, apart from vector operations, only multiplications with \mathbf{B} . The vector \mathbf{r} can in principle be determined to high accuracy. This, however, may require many multiplications with \mathbf{B} and hence may be very expensive. Therefore, the action of \mathbf{B}^{-1} is approximated to low accuracy, by performing only a few steps with an iterative solution method. The number of iterations is controlled by NINNER. The subspace generated in this way is not a Krylov subspace and the basis vectors are not the residuals (A.19) but only approximations to it. As a consequence they are not perfectly \mathbf{B} -orthogonal. The orthogonalization has to be done explicitly.

The complete algorithm can be summarized as follows.

- (i) Choose a starting vector \mathbf{v} .
- (ii) Compute $\mathbf{B}\mathbf{v}$, \mathbf{B} -normalize \mathbf{v} .
- (iii) Repeat the steps (iv)–(x) NITERL times.
- (iv) Compute $\mathbf{A}\mathbf{V}$, $\mathbf{V}^T\mathbf{A}\mathbf{V}$
- (v) Solve small eigenproblem $\mathbf{V}^T\mathbf{A}\mathbf{V}\mathbf{y} = \theta\mathbf{y}$.
- (vi) Select Ritz value θ and \mathbf{y} .
- (vii) Compute Ritz vector $\mathbf{u} = \mathbf{V}\mathbf{y}$ and residual $\tilde{\mathbf{r}} = \mathbf{A}\mathbf{V}\mathbf{y} - \theta\mathbf{B}\mathbf{V}\mathbf{y}$.
- (viii) Compute approximately $\mathbf{v} = \mathbf{B}^{-1}\tilde{\mathbf{r}}$ with the CR-method.
- (ix) \mathbf{B} -orthonormalize new \mathbf{v} against \mathbf{V} .
- (x) Expand \mathbf{V} with the resulting vector.

The matrix \mathbf{V} contains the basis for the search space, the vector \mathbf{v} contains the new basis vector and (\mathbf{u}, θ) is an approximate eigenpair. In step (vi) the pair with the largest θ is selected because only the dominant part of the spectrum is of interest. However, if the eigenpair approximation reaches a certain accuracy ε (XKAPA in namelist NAMLCZ), i.e., $\tilde{\mathbf{r}} = \mathbf{A}\mathbf{u} - \theta\mathbf{B}\mathbf{u} \leq \varepsilon$, a smaller θ is selected. In step (viii) a few CR steps are performed to approximate the action of \mathbf{B}^{-1} . In step (ix), the Modified Gram–Schmidt procedure is used for reasons of numerical stability. For a more detailed description of the Jacobi–Davidson algorithm, the reader is referred to [Sleijpen and van der Vorst \(1996\)](#)

Chapter 2

Computational details: initial perturbations

Table of contents

- 2.1 Introduction
- 2.2 Singular vectors
 - 2.2.1 The singular vector code
 - 2.2.2 Computation of singular vectors
- 2.3 Initial perturbation component based on singular vectors
- 2.4 EDA component of the initial perturbations

2.1 INTRODUCTION

For a description of the evolution of the ECMWF Ensemble Prediction System (EPS), the reader is referred to [Molteni *et al.* \(1996\)](#), [Buizza *et al.* \(1998, 1999a, 2003, 2007\)](#), [Leutbecher and Palmer \(2008\)](#) and [Buizza *et al.* \(2008\)](#). As mentioned in [Section 1.1](#), for each initial date, an ECMWF ensemble comprises one ‘control’ forecast, which is a forecast started from the operational analysis, and N_{ens} perturbed forecasts. The initial conditions for the perturbed integrations are constructed by adding to the operational analysis N_{ens} perturbations. These perturbations are determined from perturbations originating from the Ensemble of Data Assimilations (EDA) and from the leading singular vectors. The initial condition perturbations are constructed in such a way that their ensemble mean vanishes. This ensures that the ensemble initial conditions are always centred on the operational analysis. We begin with a description of the singular vector perturbations. The EDA perturbations are described in [section 2.4](#).

2.2 SINGULAR VECTORS

The part of the initial perturbations that is based on singular vectors is constructed with a Gaussian sampling technique ([Leutbecher and Palmer, 2008](#)). The sampling uses the leading singular vectors of each of the following sets of singular vectors:

- (i) Initial 50 leading northern hemisphere singular vectors, file ‘svifs’.
- (ii) Initial 50 leading southern hemisphere singular vectors, file ‘svifss’.
- (iii) Initial 5 leading singular vectors in up to 6 regions targeted on tropical cyclones, file(s) ‘svifs1’ to ‘svifs6’.

2.2.1 The singular vector code

The singular vector computation is called from **CUN3** in **CNT0** or from **CUN2** in **CUN1**, depending on whether the Hessian of the objective function is used or not. General routines related to the singular vector computation can be found in the directory ‘sinvect’. The technical routine needed for the Lanczos and Jacobi–Davidson algorithms is contained in the directory ‘var’ of IFS. Details of the set-up routines are given in [Table 2.1](#).

Subroutines **OPK** and **OPM** are the routines in which the main computational work of the singular vector computation takes place. The defining equation for the singular vectors ([1.2](#)) takes the form

$$\text{OPK}(\mathbf{x}) = \lambda \text{OPM}(\mathbf{x}) \quad (2.1)$$

Table 2.1 Constants in namelist `NAMLCZ` controlling the singular vector computation. Defaults refer to `LECMWF=TRUE`.

Name	Type	Purpose	Default
LANCZOS	LOGICAL	Activates singular vector computation with Lanczos algorithm (NCONF = 601)	TRUE
LJACDAV	LOGICAL	Activates singular vector computations with Jacobi–Davidson algorithm (NCONF = 131)	FALSE
L_USE_CONGRAD	LOGICAL	Use Lanczos algorithm in subroutine <code>CONGRAD</code>	TRUE
LOCNORM	LOGICAL	Switch to localize norm computation in grid space	TRUE
ALAT1	REAL	} NW corner of local area (defined by point 1)	90.0
ALON1	REAL		0.0
ALAT3	REAL	} SE corner of local area (defined by point 3)	30.0
ALON3	REAL		359.9
NLEVMIN	INTEGER	Minimum level of local area	1
NLEVMAX	INTEGER	Maximum level of local area	NLEVG
LSPTRLC0	LOGICAL	Switch to truncate in spectral space at initial (0) time	FALSE
LSPTRLC1	LOGICAL	Switch to truncate in spectral space at final (1) time	FALSE
NWTRMIN0(1)	INTEGER	Spectral coefficients with total wavenumber outside window are set to zero	0
NWTRMAX0(1)	INTEGER		NXMAX
LNEWNORMT0	LOGICAL	Switch to re-define the norm at initial time	FALSE
NEWNORMT0	INTEGER	Re-defines initial norm 1: total energy 2: kinetic energy 3: vorticity squared 4: stream function squared 5: rotational kinetic energy	1
NITERL	INTEGER	Maximum number of Lanczos or Jacob–Davidson inner iterations	70
NWEIGL	INTEGER	Number of singular vectors that are requested	50
XKAPA	REAL	Relative accuracy of RITZ value to consider a singular vector as converged	0.01
XMIN_RITZ	REAL	Smallest accepted RITZ value in <code>CONGRAD</code>	1.0
NINNER	INTEGER	Number of Jacobi–Davidson inner iterations	2
NJDSTOP	INTEGER	Value of NSTOP when LJACDAV = TRUE	144
LEVOLC	LOGICAL	Switch to evolve singular vectors	TRUE
NEIGEVO	INTEGER	Number of singular vectors to evolve	35
NLANTYPE	INTEGER	Determines type of singular vectors 1: energy type norms are used 2 and 3: obsolete 4: same as 1 but now NCONF = 131 5: Hessian is used at initial time 6: for computing eigensystem of the Hessian	1
LSYMCHECK	LOGICAL	Switch to activate symmetry test for operator OPK	FALSE
L_SUBSPACE_SVS	LOGICAL	Compute singular vectors in subspace orthogonal to first <code>N_DIM_SUBSPACE</code> vectors in file ‘sv_subspace’	FALSE
N_DIM_SUBSPACE	INTEGER	Number N_{sub} of vectors in ‘sv_subspace’ used to define subspace	
LSCALC	LOGICAL	Write inner product coefficients into grib-file ‘scalw’	FALSE
LRENORMALIZE	LOGICAL	Re-normalise initial singular vectors using inner product defined by ‘suscal’	FALSE

The routine `SULCZ` defines the constants as listed in Table 2.1 and determines the configuration of the singular vector computation.

The routine **OPM** is the identity in case a simple energy norm is used at initial time, or it is equal to the Hessian of the 4D-Var objective function. In the routine **OPK**, the propagators of the tangent and adjoint model are evaluated. Depending on the setting of the constants in **NAMLCZ**, additional operators may be active, such as **SPTRLCZTL** when **LSPTRLC0** = TRUE. It truncates the state vector in spectral space by setting all harmonic coefficients with total wavenumber smaller than **NWTRMIN0**, or larger than **NWTRMAX0**, to zero at initial time.

2.2.2 Computation of singular vectors

The computation of singular vectors for the EPS is organised in the following tasks in family (/mc/main/HH/sv). Task names are given in parentheses.

- (i) Retrieval of the 6-hour forecast which is used to initialise the singular vector trajectory (*getini*).
- (ii) Interpolation of the forecast to T42L91, the resolution of the singular vectors (*inidata_sv*).
- (iii) Computation of the extra-tropical initial singular vectors for the southern (*sh/sv*) and northern (*nh/sv*) hemispheres.
- (iv) Optimisation regions for the singular vector computations targeted on tropical cyclones are determined (*targets*).
- (v) Definition of the subspace of extra-tropical singular vectors used when computing the singular vectors targeted on a tropical cyclone (*subspace*).
- (vi) Computation of up to six sets of singular vectors targeted on tropical cyclones (*tc1/sv*), (*tc2/sv*), ... (*tc6/sv*).

At the time of revising this documentation (April 2014), the singular vector resolution is T42L91.

The nonlinear trajectory which defines the tangent-linear system is started from a 6-hour forecast from the delayed-cutoff stream. The use of a slightly less accurate trajectory does not significantly alter the singular vector structure and does not compromise the probabilistic skill of the EPS ([Leutbecher, 2005](#)). It has the advantage that more resources can be devoted to the singular vector computation and that the nonlinear forecasts can be started as soon as the final analysis is available.

For each hemisphere, the leading 50 singular vectors are computed. The tangent-linear model uses an adiabatic version of the forecast model (apart from vertical diffusion and surface friction).

Initial EPS perturbations in the tropics are included since cycle Cy24r3 (introduced operationally in January 2002). The leading 5 singular vectors are computed in each of up to 6 target areas. Each tropical depression/storm (WMO class ≥ 1) reported on the GTS is potentially assigned its own optimisation region. When the tropical depression/storm could be tracked in the EPS run 12 hours before the initial time, the track information is used to determine the optimisation region; otherwise the optimisation region is centred on the reported position of the tropical storm. When the procedure generates more than 6 target regions, the regions that overlap the most or are closest to each other are merged. In addition, regions with a very large overlap are merged. If no tropical storm is present in the Caribbean region an additional optimisation region in the Caribbean is specified ($0^\circ - 25^\circ\text{N}$ and $100^\circ - 60^\circ\text{W}$). The computation of the singular vectors targeted on tropical cyclones uses a diabatic version of the tangent-linear model; i.e. large-scale condensation and cumulus convection are represented in the tangent-linear model ([Barkmeijer *et al.*, 2001](#); [Puri *et al.*, 2001](#)).

The computation is triggered for tropical cyclones located between 40°S – 40°N . Therefore, the optimisation regions can significantly overlap with the optimisation region of the extra-tropical singular vector computation. In order to avoid a duplication of perturbations present in the subspace of the extra-tropical singular vectors, the singular vectors targeted on a tropical cyclone are computed in the subspace orthogonal to the space spanned by the leading 50 extra-tropical singular vectors ([Leutbecher, 2007](#)).

2.3 INITIAL PERTURBATION COMPONENT BASED ON SINGULAR VECTORS

The perturbations of the initial conditions are obtained from the singular vectors via a multivariate Gaussian sampling technique described in more detail by [Leutbecher and Palmer \(2008\)](#). Preliminary experimentation with an earlier version of the Gaussian sampling software is reported by [Ehrendorfer and Beck \(2003\)](#).

The generation of the ensemble initial perturbations consists of 3 steps. Task names are given in parentheses.

- (i) retrieval of the estimate of analysis error (getea).
- (ii) singular vector retrieval and pre-processing (getsvs).
- (iii) generation of initial perturbations (rot). The initial condition perturbations are written to a grib-file 'pert.grib' and are later archived in MARS (task lag/ ../archive/icp/ml).

Hereafter a brief description of each step is given.

The analysis error estimate is retrieved and smoothed in task (mc/sv/getea). The analysis error estimate is based on EDA variances. The standard deviation is retrieved on all model levels on a reduced Gaussian grid corresponding to the singular vector resolution. To avoid spuriously small local values of the analysis error standard deviation, the fields are smoothed by truncation to total wavenumber ≤ 21 .

The linear combination of the singular vectors into initial perturbations is done in task (mc/sv/rot) The relevant shell-script is `sample-svs` in scripts/gen. The Gaussian sampling is performed in the following three steps

- (i) Computation of the standard deviation BETA of the sampled Gaussian distribution for each set of singular vectors. This happens by comparing the singular vectors with an estimate of analysis error standard deviation provided by the EDA. See program `aev_norm` in prepdata/mc_tools.
- (ii) Generation of coefficients for the Gaussian sampling. See program `gen_sv_coeff` in prepdata/mc_tools.
- (iii) Linear combination of singular vectors. See program `sv_lin_combi` in prepdata/mc_tools.

The scaling of the width of the Gaussian distribution is performed independently for each set of singular vectors. A standard deviation β of the Gaussian distribution to be sampled is determined as follows. The singular vectors are compared with an estimate of the analysis error standard deviation using an analysis error variance norm. This is defined as the L^2 -norm of the perturbation scaled by the estimate of the analysis error standard deviation. For the re-forecasts, this estimate of the analysis error standard deviation is provided by the EDA of ERA5. In the real-time forecasts, scaled analysis error standard deviations obtained from the EDA (mars type=ses) are used as an estimate of the analysis error standard deviation. The summation in the norm extends over the entire model grid and involves the horizontal wind components, temperature and the logarithm of surface pressure, i.e. the variables defining the dry model state in grid point space. The standard deviation of the Gaussian for a set of singular vectors is set to

$$\beta = \gamma / \bar{\kappa}, \quad (2.2)$$

where $\bar{\kappa}$ denotes the average analysis error variance norm for the set of singular vectors. The parameter γ is determined empirically to yield adequate ensemble dispersion. Presently, the EPS uses $\gamma = 0.0175$ for all sets of singular vectors. The reforecasts use $\gamma = 0.013$ as the ERA5 EDA analysis error estimate is different from that of the real-time EDA.

The scaling factor γ for the singular vector perturbation amplitude is determined by SHELL-variables: `EPGAMMA`, `EPGAMMA_TC2INI`. [Table 2.2](#) describes how γ is set for each set of singular vectors depending on the two variables.

The coefficients for each set of singular vectors are generated by a call to program `gen_sv_coeff`. For each singular vector j and each odd member k random coefficients α_{jk} are drawn from the Gaussian distribution with mean zero and standard deviation β . A Gaussian distribution has no compact support,

Table 2.2 SHELL-variables determining the scaling parameter γ which controls the standard deviation of the sampled Gaussian distribution according to Eq. (2.2).

γ	singular vector sets	singular vector files
EPSGAMMA	initial extra-tropical SVs	svifs, svifss
EPSGAMMA * EPSGAMMA_TC2INI	initial SVs targeted on TCs	svifs1, ..., svifs6

i.e. the coefficients can become arbitrarily large although this is unlikely. In order to avoid numerical instabilities, due to excessively large perturbation amplitudes the coefficients are limited to the range $[-3\beta, +3\beta]$.

The singular vectors are linearly combined using program `sv_lin_combi`. The linear combination is performed in spectral space using the truncation of the singular vector computation. For each set of singular vectors, the singular vectors and the previously generated coefficients are read. The perturbations are written to a single file `pert.grib`. The perturbations are then transferred to the FDB as `type=icp` (initial condition perturbation).

The final step in generating the perturbed initial conditions consists of adding the singular vector component of the initial perturbation to the analyses that have been perturbed with the EDA-based perturbations. The perturbations based on singular vectors are added in tasks `pert_ic/NN/pertinic`. Here NN refers to the EPS member number. The addition is performed with program `add_pert`.

2.4 EDA COMPONENT OF THE INITIAL PERTURBATIONS

The EDA perturbations are based on differences between a perturbed EDA member and the EDA mean. The perturbations are computed from 6-hour forecasts as a proxy for a sample of analysis errors because the EDA is scheduled in the operational system to run in delayed mode in order to guarantee sufficient computational resources for the EDA (Isaksen *et al.*, 2010).

Since June 2019, the EDA contains $N_{\text{EDA}} = 50$ perturbed analyses (Lang *et al.*, 2019). This provides a unique EDA initial perturbation for each ensemble forecast

$$\mathbf{x}'_k = \mathbf{x}_k - \bar{\mathbf{x}}$$

with $k = 1, \dots, 50$ and $\mathbf{x}_j, \bar{\mathbf{x}}$ denoting the j -th perturbed member and the mean of all perturbed members of the EDA, respectively.

Now, the tasks are described that generate the EDA perturbations. The tasks are grouped in three families. In the first family, the high-resolution analysis that defines the centre of the EPS initial condition distribution is retrieved at full resolution (T_{Co}1279L137) from MARS and interpolated to the EPS resolution (Tasks `inigroup/an/getini` and `inidata`). In the second family (`inigroup/get_eda`), the EDA data is retrieved from MARS and interpolated to the resolution of the EPS (T_{Co}639L91, Tasks `get_eda/NNN/getini` and `inidata`). In addition, the mean of the EDA forecasts and the EDA perturbations are computed in task `get_eda/eda_mean` using program `comp_mean_pert`. In the third family (`inigroup/eda_pert`), the EDA perturbations are added to the centre analysis. Tasks `eda_pert/NNN/trans.an` generate the perturbed analyses $\mathbf{x}_c + \mathbf{x}'_{\text{NNN}}$. Here \mathbf{x}_c refers to the centre-analysis. Program `add_pert` sums unperturbed analysis and EDA perturbations. The perturbed surface fields are then constrained via the program `adjust_pertsfc` to physical values and to be consistent with the HTESSSEL IFS surface parametrisation scheme (see Part IV, Chapter 7).

The generation of the perturbed analyses can proceed even if some EDA members are not available. Tasks `get_eda/get/NNN/edamemberok` and `get_eda/get/check.edamemberok` generate the file `file_eda_list_ok`, which contains a list with the numbers of the available EDA members. If one or more perturbed EDA members are unavailable, N_{EDA} is reduced accordingly.

Chapter 3

Computational details: non-linear integrations

Table of contents

[3.1 Introduction](#)

3.1 INTRODUCTION

Since 27 June 2023, the model resolution is TCo1279L137 between forecast day 0 and 15 for the medium-range ensemble and TCo319L137 between forecast day 0 and 46 for the extended-range ensemble. The TCo1279 and TCo319 resolutions use time steps of 7.5 min and 20 min, respectively. The medium-range ensemble has 50+1 members while the extended-range/monthly ensemble has 100+1 members. Both ensembles run daily, the medium-range ensemble is initialised at 00 and 12 UTC and the extended-range/monthly ensemble is initialised at 00 UTC.

Both the medium-range and the extended-range forecasts are initialised from step $t = 0$ h. This configuration with two separate ensembles for medium-range and extended-range supersedes the merged EPS/monthly configuration (see [Buizza *et al.* \(2007\)](#) and [Vitart *et al.* \(2008\)](#)), which was operational between 11 March 2008 and 27 June 2023. [Buizza *et al.* \(2003\)](#) describe the benefits of earlier increases in the spatial resolution for the EPS. All nonlinear forecast use a single precision version of the IFS (32-bit accuracy for floating point numbers instead of 64-bit accuracy). Single precision was introduced on 11 May 2021 and permitted an increase of the number of vertical levels in the ensemble from 91 to 137 without requiring more computational resources ([Lang *et al.*, 2021](#)).

The ocean model is NEMO (see [Madec, 2008](#)) version 3.4.1 in the ORCA025 configuration (1/4 degree horizontal resolution) and 75 levels in the vertical. The LIM2 dynamic-thermodynamic sea ice component is active and uses a viscous-plastic rheology. The model timestep of NEMO is 20 minutes, the sea ice component is called every third timestep (once an hour). Since cycle Cy40r1 the ocean-atmosphere coupling has been from day 0, instead of from day 10 as in the previous cycles. NEMO is coupled to IFS every hour using a single executable framework ([Mogensen *et al.*, 2012b](#)). The sea surface temperature (SST), zonal and meridional surface currents and sea ice cover are coupled to the IFS. The ocean initial conditions come from the near real-time component of the operational ocean analysis (NEMOVAR, see [Mogensen *et al.*, 2012a](#)) or from the Ocean ReAnalysis System 5 (ORAS5, see [Zuo *et al.*, 2017](#)) for re-forecasts. In the extratropics, the atmosphere is forced by the SST from the ocean model plus an additional term which is the difference between the high resolution SST from OSTIA and the low resolution SST from the ocean analysis at step 0 during the first 5 days of the forecast. After day 5, this additional term is relaxed to reach 0 by day 9. This additional term ensures that the SSTs during the first days of the forecasts still contains the high resolution information of the OSTIA SST analysis. In the tropics, the atmosphere is forced directly by the SST from the ocean model.

Two types of ensemble forecasts are currently run: the control forecast and the perturbed forecasts. The control forecast family includes four tasks: task `cf/getinileg` copies the initial conditions in the forecast working directory, while task `cf/modeleps_nemo` performs the integration. The family `oceanini` prepares the ocean initial conditions. Tasks `modeleps_tidy` deals with the restart data for the ocean model. Control forecast data are archived in MARS (the ECMWF Meteorological Archival and Retrieval System) with `type=cf`, `stream=enfo` (medium-range) and `type=cf`, `stream=eefo` (extended-range).

The perturbed forecast family `pf` includes 50 (100) sub-families, named `pf/001`, `pf/002`, ... Each sub-family includes the same tasks as the control forecast: task `pf/NNN/getinileg` copies the perturbed

initial conditions in the forecast working directory, while `pf/NNN/modeleps_nemo` performs the integration. The family `oceanini` prepares the ocean initial conditions. Tasks `modeleps_tidy` and `sppt2fdb` deal with the restart data for the ocean model and the SPPT scheme, respectively. Perturbed forecast data are archived in MARS with `type=pf, stream=enfo` (medium-range) and `type=pf, stream=eefo` (extended-range). The medium-range reforecasts are archived in MARS in `stream=enfh` while the extended-range reforecasts are archived in `stream=eefh`.

References

- Baran, S., Leutbecher, M., Szabó, M. and Ben Bouallègue, Z. (2019). Statistical post-processing of dual-resolution ensemble forecasts. *Q. J. R. Meteorol. Soc.*, **145**, 1705–1720, doi:10.1002/qj.3521.
- Barkmeijer, J., Buizza, R., Palmer, T. N., Puri, K. and Mahfouf, J.-F. (2001). Tropical singular vectors computed with linearized diabatic physics. *Q. J. R. Meteorol. Soc.*, **127**, 685–708.
- Barkmeijer, J., van Gijzen, M. and Bouttier, F. (1998). Singular vectors and estimates of the analysis error covariance metric. *Q. J. R. Meteorol. Soc.*, **124**, 1695–1713.
- Berner, J., Shutts, G. J., Leutbecher, M. and Palmer, T. N. (2009). A spectral stochastic kinetic energy backscatter scheme and its impact on flow-dependent predictability in the ECMWF ensemble prediction system. *J. Atmos. Sci.*, **66**, 603–626.
- Bourke, W., Buizza, R. and Naughton, M. (2005). Performance of the ECMWF and the BoM ensemble systems in the southern hemisphere. *Mon. Wea. Rev.*, **132**, 2338–2357.
- Buizza, R. (1994). Localization of optimal perturbations using a projection operator. *Q. J. R. Meteorol. Soc.*, **120**, 1647–1682.
- Buizza, R., Barkmeijer, J., Palmer, T. N. and Richardson, D. S. (1999a). Current status and future developments of the ECMWF ensemble prediction system. *Meteorol. Appl.*, **6**, 1–14.
- Buizza, R., Bidlot, J. R., Wedi, N., Fuentes, M., Hamrud, M., Holt, G. and Vitart, F. (2007). The new ECMWF VAREPS (variable resolution ensemble prediction system). *Q. J. R. Meteorol. Soc.*, **133**, 681–695.
- Buizza, R., Houtekamer, P. L., Toth, Z., Pellerin, G., Wei, M. and Zhu, Y. (2005). A comparison of the ECMWF, MSC and NCEP global ensemble prediction systems. *Mon. Wea. Rev.*, **133**, 1076–1097.
- Buizza, R., Leutbecher, M. and Isaksen, L. (2008). Potential use of an ensemble of analyses in the ECMWF ensemble prediction system. *Q. J. R. Meteorol. Soc.*, **134**, 2051–2066.
- Buizza, R., Miller, M. and Palmer, T. N. (1999b). Stochastic representation of model uncertainties in the ECMWF ensemble prediction system. *Q. J. R. Meteorol. Soc.*, **125**, 2887–2908.
- Buizza, R. and Palmer, T. N. (1995). The singular vector structure of the atmosphere global circulation. *J. Atmos. Sci.*, **52**, 1434–1456.
- Buizza, R., Petroliaigis, T., Palmer, T. N., Barkmeijer, J., Hamrud, M., Hollingsworth, A., Simmons, A. and Wedi, N. (1998). Impact of model resolution and ensemble size on the performance of an ensemble prediction system. *Q. J. R. Meteorol. Soc.*, **124**, 1935–1960.
- Buizza, R., Richardson, D. S. and Palmer, T. N. (2003). Benefits of increased resolution in the ECMWF ensemble system and comparison with poor-man's ensembles. *Q. J. R. Meteorol. Soc.*, **129**, 1269–1288.
- Ehrendorfer, M. and Beck, A. (2003). Singular vector-based multivariate normal sampling in ensemble prediction. *ECMWF Tech. Memo. No. 416*.
- Ehrendorfer, M. and Tribbia, J. J. (1997). Optimal prediction of forecast error covariances through singular vectors. *J. Atmos. Sci.*, **53**, 286–313.

- Gelaro, R., Buizza, R., Palmer, T. N. and Klinker, E. (1998). Sensitivity analysis of forecast errors and the construction of optimal perturbations using singular vectors. *J. Atmos. Sci.*, **55**, 1012–1037.
- Golub, G. H. and van Loan, C. F. (1983). *Matrix Computation*. North Oxford Academic Publ. Co. Ltd.
- Hagedorn, R. (2008). Using the ECMWF reforecast dataset to calibrate EPS forecasts. *ECMWF Newsletter No. 117*, pp. 8–13.
- Hagedorn, R., Buizza, R., Hamill, M. T., Leutbecher, M. and Palmer, T. N. (2012). Comparing TIGGE multi-model forecasts with re-forecast calibrated ECMWF ensemble forecasts. *Q. J. R. Meteorol. Soc.*, **138**, 1814–1827.
- Harrison, M. S., Palmer, T. N., Richardson, D. and Buizza, R. (1999). Analysis and model dependencies in medium-range ensembles: Two transplant case studies. *Q. J. R. Meteorol. Soc.*, **126**, 2487–2515.
- Hersbach, H., Bell, B., Berrisford, P., Horányi, A., Sabater, J. M., Nicolas, J., Radu, R., Schepers, D., Simmons, A., Soci, C. and Dee, D. (2019). Global reanalysis: goodbye ERA-Interim, hello ERA5. *ECMWF Newsletter No. 159 - Spring 2019*, doi:10.21957/vf291hehd7, URL <https://www.ecmwf.int/node/19001>.
- Hoskins, B. J., Buizza, R. and Badger, J. (2000). The nature of singular vector growth and structure. *Q. J. R. Meteorol. Soc.*, **126**, 1565–1580.
- Houtekamer, P. L., Lefaiivre, L. and Derome, J. (1996a). The RPN ensemble prediction system. In *Proc. ECMWF Seminar on Predictability*, Vol. II, pp. 121–146, 4–8 September 1995, Reading, UK.
- Houtekamer, P. L., Lefaiivre, L., Derome, J., Ritchie, H. and Mitchell, H. L. (1996b). A system simulation approach to ensemble prediction. *Mon. Wea. Rev.*, **124**, 1225–1242.
- Isaksen, L. M. B., R. Buizza, M. F., Haseler, J., Leutbecher, M. and Raynaud, L. (2010). Ensemble of data assimilations at ECMWF. *Technical Report 636*, ECMWF, Reading, UK.
- Lang, S., Holm, E., Bonavita, M. and Tremolet, Y. (2019). A 50-member ensemble of data assimilations. *ECMWF Newsletter No. 158 - Winter 2018/19*, URL <https://www.ecmwf.int/node/18821>.
- Lang, S. T. K., Dawson, A., Diamantakis, M., Dueben, P., Hatfield, S., Leutbecher, M., Palmer, T., Prates, F., Roberts, C. D., Sandu, I. and Wedi, N. (2021). More accuracy with less precision. *Q. J. R. Meteorol. Soc.*, **147**(741), 4358–4370, doi:<https://doi.org/10.1002/qj.4181>.
- Lawrence, A. R., Leutbecher, M. and Palmer, T. N. (2009). The characteristics of hessian singular vectors using an advanced data assimilation scheme. *Q. J. R. Meteorol. Soc.*, **135**, 1117–1132.
- Leutbecher, M. (2005). On ensemble prediction using singular vectors started from forecasts. *Mon. Wea. Rev.*, **133**, 3038–3046.
- Leutbecher, M. (2007). On the representation of initial uncertainties with multiple sets of singular vectors optimised for different criteria. *Q. J. R. Meteorol. Soc.*, **133**, 2045–2056.
- Leutbecher, M. and Ben Bouallègue, Z. (2020). On the probabilistic skill of dual-resolution ensemble forecasts. *Q. J. R. Meteorol. Soc.*, **146**, 707–723, doi:10.1002/qj.3704.
- Leutbecher, M. and Lang, S. T. K. (2014). On the reliability of ensemble variance in subspaces defined by singular vectors. *Q. J. R. Meteorol. Soc.*, **140**, 1453–1466, doi:10.1002/qj.2229.
- Leutbecher, M., Lock, S.-J., Ollinaho, P., Lang, S. T. K., Balsamo, G., Bechtold, P., Bonavita, M., Christensen, H. M., Diamantakis, M., Dutra, E., English, S., Fisher, M., Forbes, R. M., Goddard, J., Haiden, T., Hogan, R. J., Juricke, S., Lawrence, H., MacLeod, D., Magnusson, L., Malardel, S., Massart, S., Sandu, I., Smolarkiewicz, P. K., Subramanian, A., Vitart, F., Wedi, N. and Weisheimer, A. (2017). Stochastic representations of model uncertainties at ECMWF: state of the art and future vision. *Q. J. R. Meteorol. Soc.*, **143**, 2315–2339, doi:10.1002/qj.3094.
- Leutbecher, M. and Palmer, T. N. (2008). Ensemble forecasting. *J. Comp. Phys.*, **227**, 3515–3539.

- Lock, S.-J., Lang, S. T. K., Leutbecher, M., Hogan, R. J. and Vitart, F. (2019). Treatment of model uncertainty from radiation by the stochastically perturbed parametrization tendencies (sppt) scheme and associated revisions in the ecmwf ensembles. *Quarterly Journal of the Royal Meteorological Society*, **145**(S1), 75–89, doi:<https://doi.org/10.1002/qj.3570>.
- Madec, G. (2008). *NEMO reference manual, ocean dynamics component: NEMO_OPA. Preliminary version*. Institut Pierre-Simon Laplace (IPSL), France, note du pole de modelisation 27.
- Mogensen, K., Balmaseda, M. and Weaver, A. (2012a). The NEMOVAR ocean data assimilation system as implemented in the ECMWF ocean analysis for System 4. *Tech. Memo. 668*, ECMWF, available at www.ecmwf.int/publications/library/do/references/show?id=90389.
- Mogensen, K., Keeley, S. and Towers, P. (2012b). Coupling of the NEMO and IFS models in a single executable. *Tech. Memo. 673*, ECMWF, available at www.ecmwf.int/publications/library/do/references/show?id=90460.
- Molteni, F., Buizza, R., Palmer, T. N. and Petroliagis, T. (1996). The ECMWF Ensemble Prediction System: methodology and validation. *Q. J. R. Meteorol. Soc.*, **122**, 73–119.
- Mureau, F., Molteni, F. and Palmer, T. N. (1993). Ensemble prediction using dynamically conditioned perturbations. *Q. J. R. Meteorol. Soc.*, **119**, 299–298.
- Palmer, T. N., Buizza, R., Doblas-Reyes, F., Jung, T., Leutbecher, M., Shutts, G. J., Steinheimer, M. and Weisheimer, A. (2009). Stochastic parameterization and model uncertainty. *ECMWF Tech. Memo. No. 598*, pp. 1–42.
- Palmer, T. N., Gelaro, R., Barkmeijer, J. and Buizza, R. (1998). Singular vectors, metrics and adaptive observations. *J. Atmos. Sci.*, **55**, 633–653.
- Palmer, T. N., Molteni, F., Mureau, R., Buizza, R., Chapelet, P. and Tribbia, J. (1993). Ensemble Prediction. In *Proc. of the ECMWF Seminar on Validation of Models over Europe: Vol. 1*, pp. 21–66, 7–11 September 1992, Reading, UK.
- Park, Y.-Y., Buizza, R. and Leutbecher, M. (2008). TIGGE: preliminary results on comparing and combining ensembles. *ECMWF Tech. Memo. No. 548*.
- Puri, K., Barkmeijer, J. and Palmer, T. N. (2001). Ensemble prediction of tropical cyclones using targeted diabatic singular vectors. *Q. J. R. Meteorol. Soc.*, **127**, 709–734.
- Rabier, F., Klinker, E., Courtier, P. and Hollingsworth, A. (1996). Sensitivity of forecast errors to initial conditions. *Q. J. R. Meteorol. Soc.*, **122**, 121–150.
- Sleijpen, G. L. G. and van der Vorst, H. A. (1996). A Jacobi–Davidson iteration method for linear eigenvalue problems. *SIAM J. Matrix Anal. Appl.*, **17**, 401–425.
- Toth, Z. and Kalnay, E. (1993). Ensemble forecasting at NMC: the generation of initial perturbations. *Bull. Am. Meteorol. Soc.*, **74**, 2317–2330.
- Toth, Z. and Kalnay, E. (1997). Ensemble forecasting at NCEP and the breeding method. *Mon. Wea. Rev.*, **125**, 3297–3319.
- Trevisan, A., Pancotti, F. and Molteni, F. (2001). Ensemble prediction in a model with flow regimes. *Q. J. R. Meteorol. Soc.*, **127**, 343–358.
- Vitart, F. (2004). Monthly forecasting at ECMWF. *Mon. Wea. Rev.*, **132**, 2671–2779.
- Vitart, F., Balsamo, G., Bidlot, J.-R., Lang, S., Tsonevsky, I., Richardson, D. and Alonso-Balmaseda, M. (2019). Use of ERA5 to initialize ensemble re-forecasts. *ECMWF Tech. Memo.*, **841**, doi:10.21957/w8i57wuz6, URL <https://www.ecmwf.int/node/18872>.
- Vitart, F., Buizza, R., Balmaseda, M. A., Balsamo, G., Bidlot, J., Bonet, A., Fuentes, M., Hofstadler, A., Molteni, F. and Palmer, T. N. (2008). The new VAREPS-monthly forecasting system: a first step towards seamless prediction. *Q. J. R. Meteorol. Soc.*, **134**, 1789–1799.

Zsoter, E., Buizza, R. and Richardson, D. (2009). Jumpiness of the ECMWF and UK met office EPS control and ensemble-mean forecasts. *Mon. Wea. Rev.*, **137**, 3823–3836.

Zuo, H., Balmaseda, M. A., Boisseson, E. and Hirahara, S. (2017). A new ensemble generation scheme for ocean analysis. *Tech. Memo. 795*, ECMWF.